

This article was downloaded by: [31.29.35.203]

On: 21 May 2015, At: 06:58

Publisher: Taylor & Francis

Informa Ltd Registered in England and Wales Registered Number: 1072954 Registered office: Mortimer House, 37-41 Mortimer Street, London W1T 3JH, UK



International Journal of Crashworthiness

Publication details, including instructions for authors and subscription information:
<http://www.tandfonline.com/loi/tcrs20>

Analytical, experimental and numerical study of a graded honeycomb structure under in-plane impact load with low velocity

S.A. Galehdari^a, M. Kadkhodayan^a & S. Hadidi-Moud^a

^a Department of Mechanical Engineering, Ferdowsi University of Mashhad, Mashhad, Iran
Published online: 11 Mar 2015.



CrossMark

[Click for updates](#)

To cite this article: S.A. Galehdari, M. Kadkhodayan & S. Hadidi-Moud (2015) Analytical, experimental and numerical study of a graded honeycomb structure under in-plane impact load with low velocity, International Journal of Crashworthiness, 20:4, 387-400, DOI: [10.1080/13588265.2015.1018739](https://doi.org/10.1080/13588265.2015.1018739)

To link to this article: <http://dx.doi.org/10.1080/13588265.2015.1018739>

PLEASE SCROLL DOWN FOR ARTICLE

Taylor & Francis makes every effort to ensure the accuracy of all the information (the "Content") contained in the publications on our platform. However, Taylor & Francis, our agents, and our licensors make no representations or warranties whatsoever as to the accuracy, completeness, or suitability for any purpose of the Content. Any opinions and views expressed in this publication are the opinions and views of the authors, and are not the views of or endorsed by Taylor & Francis. The accuracy of the Content should not be relied upon and should be independently verified with primary sources of information. Taylor and Francis shall not be liable for any losses, actions, claims, proceedings, demands, costs, expenses, damages, and other liabilities whatsoever or howsoever caused arising directly or indirectly in connection with, in relation to or arising out of the use of the Content.

This article may be used for research, teaching, and private study purposes. Any substantial or systematic reproduction, redistribution, reselling, loan, sub-licensing, systematic supply, or distribution in any form to anyone is expressly forbidden. Terms & Conditions of access and use can be found at <http://www.tandfonline.com/page/terms-and-conditions>

Analytical, experimental and numerical study of a graded honeycomb structure under in-plane impact load with low velocity

S.A. Galehdari, M. Kadkhodayan* and S. Hadidi-Moud

Department of Mechanical Engineering, Ferdowsi University of Mashhad, Mashhad, Iran

(Received 11 December 2014; accepted 10 February 2015)

Given the significance of energy absorption in various industries, light shock absorbers such as honeycomb structure under in-plane and out-of-plane loads have been in the core of attention. The purpose of this research is the analyses of graded honeycomb structure (GHS) behaviour under in-plane impact loading and its optimisation. Primarily, analytical equations for plateau stress and specific energy are represented, taking power hardening model (PHM) and elastic–perfectly plastic model (EPPM) into consideration. For the validation and comparison of acquired analytical equations, the energy absorption of a GHS made of five different aluminium grades is simulated in ABAQUS/CAE. In order to validate the numerical simulation method in ABAQUS, an experimental test has been conducted as the falling a weight with low velocity on a GHS. Numerical results retain an acceptable accordance with experimental ones with a 5.4% occurred error of reaction force. For a structure with a specific kinetic energy, the stress–strain diagram is achieved and compared with the analytical equations obtained. The maximum difference between the numerical and analytical plateau stresses for PHM is 10.58%. However, this value has been measured to be 38.78% for EPPM. In addition, the numerical value of absorbed energy is compared to that of analytical method for two material models. The maximum difference between the numerical and analytical absorbed energies for PHM model is 6.4%, while it retains the value of 48.08% for EPPM. Based on the conducted comparisons, the numerical and analytical results based on PHM are more congruent than EPPM results. Applying sequential quadratic programming method and genetic algorithm, the ratio of structure mass to the absorbed energy is minimised. According to the optimisation results, the structure capacity of absorbing energy increases by 18% compared to the primary model.

Keywords: graded honeycomb structure; in-plane impact load; power hardening; plateau stress; specific absorbed energy (SAE); optimisation

Nomenclature

GHS	Graded honeycomb structure	n	Strain-hardening index
A	Cross-sectional area of GHS perpendicular to loading direction	u	Strain energy per unit mass
b	Depth of GHS cell	U	Strain energy
c	Cell horizontal wall length	ub	Upper limits of the variables vector
d	Cell wall thickness	X	Optimisation design variables vector
e	Specific absorbed energy	y	Distance from neutral axis
e_f	Elongation	σ	Stress tensor
K	Coefficient of strain-hardening relation	σ_y	Yield stress
L	Height of GHS	σ_u	Ultimate stress
l	Cell inclined wall length	σ_p	Plateau stress
l_p	Plastic hinge length	ϵ_d	Locking strain
lb	Lower limits of the variable vector	ρ	Density of honeycomb structure
W	Width of the GHS	ρ_s	Density of honeycomb structure material
m	GHS mass	ρ^*	Relative density of honeycomb structure
m_c	Mass of each cell	ϵ_c	Compressive strain
M_{py}	Fully plastic moment based on EPPM	ϕ	Honeycomb cell's angle
M_{pu}	Fully plastic moment based on PHM		
M_y	Initial yielding moment		

1. Introduction

With the noticeably rapid development in automotive, transportation and aeronautics engineering, analysing the

*Corresponding author. Email: kadkhoda@um.ac.ir

energy absorption capacity in structures has become an important field of research. In the last decade, various materials and structures with high specific absorbing energy such as graded honeycomb structure (GHS) and thin vessel structures have been studied [21]. One of the most important characteristics of GHSs is that by changing the geometrical parameters of the structure such as height, thickness, cell size and inner angles, different mechanical characteristics could be obtained [1]. The most important purpose of this structure is reducing the effect of impact load by its distribution within a time period. The main characteristics of energy-absorbing cellular structures are to absorb energy in an irreversible manner, reduce reactive load, undergo repeatable deformation mode, be compact, be light in weight and have higher specific energy absorption capacity, be inexpensive and easy to install. The common forms of cellular structures are (1) open cell structures in which cells are arranged in a two-dimensional (2D) regular or irregular array and (2) closed cell structures in which plates are inter-connected and formed 3D, partially open or closed with regular- or irregular-shaped cells. Honeycomb structures are considered as one of the primary shock absorbers. These structures are widely used in automotive, aeronautics and packing industries. Scientifically speaking, banana peel which is a functionally graded material (FGM) is a type of energy absorber [18]. Moreover, the human and bird bones are natural shock absorbers. The cancellous structure of bone leads to the absorption of applied shock as well as the reduction of bearing stress in joints. Aluminium honeycomb structures are well-known energy absorbers and have wide applications in automobiles, aircrafts and packaging industries. They also provide a platform to expand knowledge of the existing uniform-wall open-cell structures to non-uniform cell-wall-graded structures [20]. Extensive research has been done in understanding the in-plane and out-of-plane behaviours of honeycombs. Deqiang et al. [7] represented a finite-element model (FEM) for analysing the behaviour of this type of structure under impact loads using LS-Dyna software. Song et al. [27] analysed the dynamic pressure behaviour of a 3D structure made of foam. An experimental test was also conducted through Voronoi arranging method. Another FE model was used by Song, where the values of plateau stress and strain energy were obtained to investigate the influence of cells shape, impact load, relative density and strain hardening on the deformation mode and plateau stress. The results showed that the values of plateau stress and energy absorption increased with the rising of cells irregularity. Asadi et al. [3] presented a simple FE model for the application of imploding in honeycomb structures. This model can be applied not only to the simple honeycomb, but also to the more complicated structures such as honeycomb structures with several layers or materials. The numerical results obtained

showed an appropriate congruence with the experimental results. Liaghat et al. [15] optimised the honeycomb structure under compression loading and an optimisation was conducted using both MATLAB software and analytical methods. The optimisation of structure cells with different geometries was also analysed. Zou et al. [29] analysed the in-plane dynamic destruction of regular honeycomb structures by FEM and compared the obtained plateau stresses by analytical and numerical methods to each other. They have also analysed different mechanisms of structure cells deformation and have represented the stress–velocity diagrams. Ajdari et al. [2] analysed the dynamic destruction behaviour and the value of energy absorption in regular, irregular and FG honeycomb structures. They studied different modes of deformation and the value of energy absorption in these structures using FEM. Mohammad-Ali et al. [20,19] simulated the behaviour of GHS under impact load and presented an analytical equation for dynamic plateau stress corresponding to high velocities. The results of analytical equation were compared to those of numerical solution. In addition, to reduce the layer thickness in the direction of panel sandwich thickness, the material hardness was also decreased. In another study, they studied the in-plane response of the graded structure under medium- and high-velocity impacts. Different critical energy-absorbing characteristics, e.g. deformation modes, collapsing mechanism, crushing stress, locking strain and total energy absorbed, have been discussed. In the above studies, the ideal elastic–perfectly plastic model (EPPM) has been used to derive the plateau stress and specific energy of structure. However, comparison of numerical and analytical results shows high difference. In the current research, in order to reduce the difference, the plateau stress and specific energy of structure are driven based on power-hardening material model. To verify the driven equation, FE analysis is executed in ABAQUS. After that, according to the driven equations, the specific energy of the structure is optimised. Papka and Kyriakides [22,23] studied the load–displacement response of hexagonal-cell aluminium honeycombs as well as circular polycarbonate honeycombs under in-plane uniaxial loading. They observed various deformation patterns (modes), which were related to the particular ratio between the components of the applied displacements or forces.

2. Banana peel: a compact energy absorber

The structures replicated from honeycombs are one of the prime candidates for reducing the impact in automobile, aerospace and packaging industries [5]. Figure 1 shows the cross sections of a banana peel. In technical terms, such kinds of materials are called FGMs. In FGM, the composition and structure gradually vary with depth, resulting in corresponding changes in the properties of the material. Observations show that such types of FGM

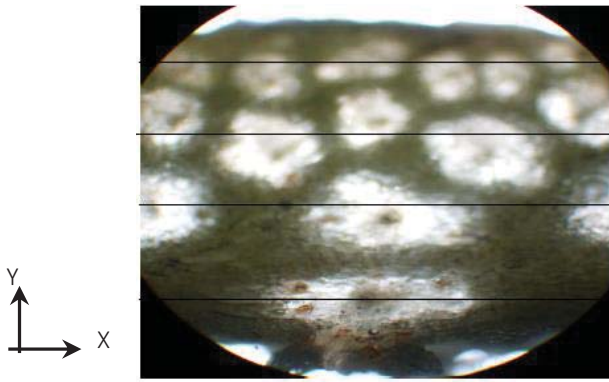


Figure 1. Cross section of a banana peel [18].

structures are highly adaptive to all boundary and loading conditions defined by their environment. For example, the interior structure of a bone has an optimised shape with respect to the direction of principal stress and the magnitude of shear stress [25]. In a banana peel, one of the main objectives is to protect the internal soft core from external impacts.

The arrangement of cells can be broken down into layers in the X -direction and the grading (variation in size) in the Y -direction (see Figure 1). Four layers can be easily identified. These layers are indicated by horizontal lines. The first layer from the top is composed of closely packed cells. The second layer is composed of bigger cells with more spacing among them. This variation in the pattern continues until the last layer, where cells are widely dispersed. The graded structure shows that the stiffness changes with thickness. According to structural mechanics, two different sized cross sections with the same shape factor have different stiffness. The larger the cross section is, the lower is the stiffness [13]. If a foreign object hits a banana peel from the top (or a banana falls on another object), the inner cells collapse first to protect the soft core. This 'collapse mechanism' would flow up and layers would continue crushing until the whole structure is compromised. It is evident that such a 'collapse mechanism' allows structures to reduce the kinetic energy of the object over a finite period of time and the overall effect is a reduction in the impact load. The presence of fluid in the cells enhances the integrity and total energy absorption capability of the structure. The widely dispersed (biggest) cells in the bottom layer do not communicate structurally with one another. This information leads to the hypothesis that the structure in a banana peel acts as a compact energy absorber. However, the banana peel structure is too complex to handle and, therefore, a few assumptions are made to redefine the structure without excessive deviation from the peel structure. It is assumed that the material is homogenous along the thickness, the cells have constant shape factor and are arranged in a uniform order. Figure 2 shows the modified peel structure and it may be

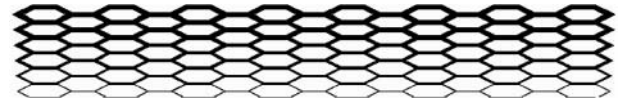


Figure 2. The modified peel structure [18].

called the GHS. The global response of the structure can be achieved by summing up the local response of individual rows. Due to the complexity of the peel structure and emphasis on extracting the cellular structure for investigating the in-plane crushing behaviour, the following assumptions are made to model the banana peel structure: (1) the cell-wall material is homogenous, (2) the shape of the cells and their aspect ratios do not vary with thickness, and (3) the effect of fluid inside the cells is ignored. In addition, the cell arrangement depicted in Figure 1 more or less stays the same in the Z -direction, which allows an in-plane 2D analysis feasible. The quasi-static and low-dynamic analysis for impact velocities up to 20 m s^{-1} show that the peel graded structure has superior energy-absorbing characteristics for a broader range of impact velocities in a restricted space as compared to regular honeycombs of constant wall thickness. A balanced response between the structure integrity and attenuation of reaction load is observed. At microscopic scale, the compacted cell shape keeps the impact effects low. A theoretical model was presented that correctly captured the crushing response of peel structure at static and low-dynamic loadings [18]. According to the represented information, the semi-honeycomb structure of the banana peel has the responsibility of protecting its core, in addition to several biological roles. Therefore, inspiring from a banana peel structure, a GHS is modelled. The integral characteristic of this type of absorber is its status of being graded. The variation of the stiffness of the structure from the hitting point to the protected body results in an increase of force transfer time. This duration, in case of being long, can be considered as a positive parameter for shock absorbers. Accordingly, a numerical, experimental and analytical study of GHS is conducted in this research.

3. Mechanics of honeycomb structure

A typical honeycomb cell with its parameters is shown in Figure 3. The behaviour of honeycomb structure under compression loading can be determined using five modules including two Young modules E_1 and E_2 , a shear module G_{12} and two Poisson coefficients ν_{12} and ν_{21} .

Honeycomb structures transform in-plane kinetic energy into strain energy by crushing the rows. This strain energy is equal to plastic hinge energy and elastic one. It should be mentioned that the elastic strain energy is neglected due to its small amount compared to the plastic one. The most important parameters characterising cellular material energy absorption properties are the plastic

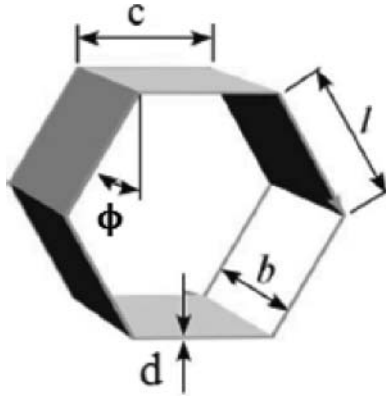


Figure 3. Honeycomb structure cell.

collapse stress generally known as the plateau stress and the relative density. The upper and lower bound theorems are used to determine the plateau stress. According to the upper bound theorem, an external load computed on the basis of an assumed mechanism, in which the forces are in equilibrium, is always greater than or equal to the true collapse load. On the other hand, the lower bound theorem says that an external load computed on the basis of an assumed distribution of internal forces, in which the forces are bounded by limit values and the forces are in equilibrium, is less than or equal to the true collapse load [8]. If a part of stress–strain diagram has a constant stress, it is called *plateau stress*. In fact, the value of plateau stress is not constant; however, its changes are negligible [16]. In deriving analytical equations, the value of σ_p is considered as constant. So far, the EPPM has been used to derive the plateau stress. In this study, due to the previously high difference between the numerical and analytical results, the power hardening model (PHM) is used. The fully plastic moment of honeycomb wall is given by

$$M_p = 2b \int_0^{\frac{d}{2}} y \sigma \, dy \quad (1)$$

Based on the EPPM, the fully plastic moment can be obtained as

$$M_{py} = \frac{b\sigma_y d^2}{4} \quad (2)$$

Considering the material model with the power hardening and by substituting $\sigma = K\varepsilon^n$ and $\varepsilon = \frac{2y}{d} \varepsilon_{\max}$ [4] in Equation (1), the corresponding fully plastic moment can be obtained as

$$M_{pu} = \frac{b\sigma_u d^2}{2(n+2)} \quad (3)$$

where σ_u is the ultimate strength of the material of structure cell. Based on upper and lower bound theorems and using Equation (2), the plastic–perfectly plastic plateau stress can

be derived [8] as

$$\sigma_p = \frac{\sigma_y d^2}{2(c + l \sin \phi) l \sin \phi} \quad (4)$$

The compressive load in the *Y*-direction is transferred to the inclined walls and they bend like a frame. The plastic analysis shows that six plastic hinges [28] are required to define the complete ‘collapse mechanism’ of a cell. Figure 4 shows the inclined wall undergoing angular rotation, ψ , with respect to its original position. An upper bound on the load acting on the wall is given by

$$P = \sigma_p (c + l \sin \phi) b \quad (5)$$

For a cantilever beam subjected to load P , the plastic hinge length l_p is determined from the ultimate moment diagram at the point of collapse. The plastic hinge length at the end of the beam is given by

$$l_p = \frac{l}{4} \left(1 - \frac{M_y}{M_p} \right) \quad (6)$$

where M_y and M_p are initial yielding and fully plastic moments, respectively. Initial yielding moment can be obtained as [26]

$$M_y = \frac{b\sigma_y d^2}{6} \quad (7)$$

Substituting Equations (3) and (7) into Equation (6), the plastic hinge length at the end of the beam for PHM is derived as

$$l_p = \frac{l}{4} \left(1 - \frac{(n+2)\sigma_y}{3\sigma_u} \right) \quad (8)$$

For $\frac{d}{l} < 0.25$, the axial and shear deflections are small compared to bending deflections. Therefore, they do not significantly affect the plateau stress and bending moment considerably [8]. Plastic hinge length itself has little effect on the load but significantly changes the deformation

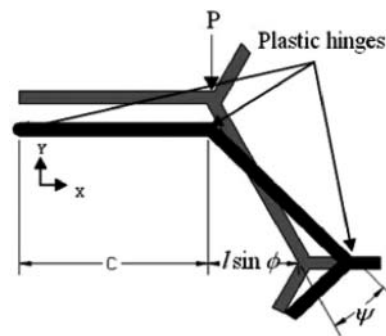


Figure 4. Plastic collapse of inclined walls in the *Y*-direction.

geometry and hence the moment arm of the bending moment [24]. Therefore, only the plastic hinge length effect was taken into account to derive the plateau stress equation. The length of the plastic hinge was obtained by observing the values of bending moment, equivalent plastic strains and von Mises stress [14,12] at the integration points of the shell elements in the FE analysis. It was found to equal half the thickness of the cell wall. Hence, the moment arm (l) is reduced to $l - d$. A lower bound on a collapse load is calculated by equating the internal negative moment on the cell wall to the external positive moment as shown in Figure 5 (Equation 9).

$$2M_p = P(l - d) \sin \phi \tag{9}$$

Substituting Equations (3) and (5) into Equation (9), the PHM plateau stress is derived as

$$\sigma_p = \left(\frac{\sigma_u}{n + 2} \right) \frac{d^2}{(c + l \sin \phi)(l - d) \sin \phi} \tag{10}$$

The corresponding locking strain based on relative density can be calculated as [8]

$$\rho = \frac{\left(\frac{d}{l}\right)\left(\frac{c}{l} + 2\right)}{2(\sin(\phi) + \frac{c}{l})\cos(\phi)} \rho_s \tag{11}$$

It is noteworthy that ρ^* is the ratio of structure cell density to the density of the material of the honeycomb structure ($\rho^* = \frac{\rho}{\rho_s}$). In the above-mentioned equation, ρ_s is the density of the material of honeycomb structure. The porosity, which in fact is the pore volume, is $1 - \frac{\rho}{\rho_s}$. This value is approximately equal to the locking strain ϵ_d as [8]

$$\epsilon_d = 1 - \rho^* = 1 - \frac{\left(\frac{d}{l}\right)\left(\frac{c}{l} + 2\right)}{2(\sin(\phi) + \frac{c}{l})\cos(\phi)} \tag{12}$$

It should be mentioned that by increasing the thickness of honeycomb cell wall, the locking strain becomes lower than that of the calculated value in the equation mentioned above; however, the exact value could be obtained through

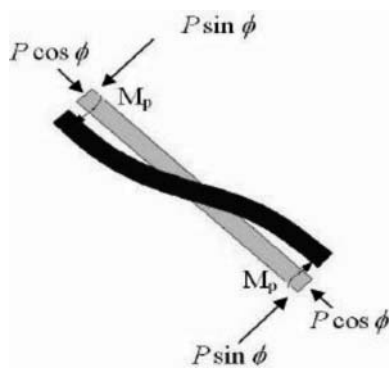


Figure 5. Internal and external bending moments on the inclined wall.

the experimental tests. The parameter ϵ_d is the strain corresponding to the end of deformation in each row. In the following, it is assumed that the absorbed energy is equal to the strain energy of the entire structure. The equation of strain energy is

$$U = \int(\int \sigma d\epsilon) dV \tag{13}$$

where σ is the stress tensor applied to the structure, ϵ is the strain tensor and V is the volume of the structure. In order to calculate the strain energy per unit volume, the area below the surface of the stress–strain diagram is found (Figure 5). Since the thickness of the cell walls is changing, the equations presented above can only capture the response of individual rows. Each row of the structure would confront deformation in plateau stress and locking strain. Therefore, considering $\sigma = \sigma_p$ and $\epsilon = \epsilon_d$ (the equal values of stress to plateau stress and strain to locking strain), strain energy per unit volume would be

$$u = \sum_{i=1}^6 \sigma_{p_i} \epsilon_{d_i} \tag{14}$$

In order to study the behaviour of the entire structure, the analytical equations of all layers can be then summed up. According to the represented analytical equations, the plateau stress and locking strain diagram have been demonstrated in Figure 6.

Based on the equations obtained, the strain energy for the entire structure can be obtained as

$$U = \int(\int \sigma_p d\epsilon_d) dV = AL \sum_{i=1}^6 \sigma_{p_i} \frac{\epsilon_{d_i}}{6} \tag{15}$$

where σ_{p_i} is the plateau stress of each row for the material model with power hardening, ϵ_{d_i} is the corresponding locking strain for each row, A is the cross section of the

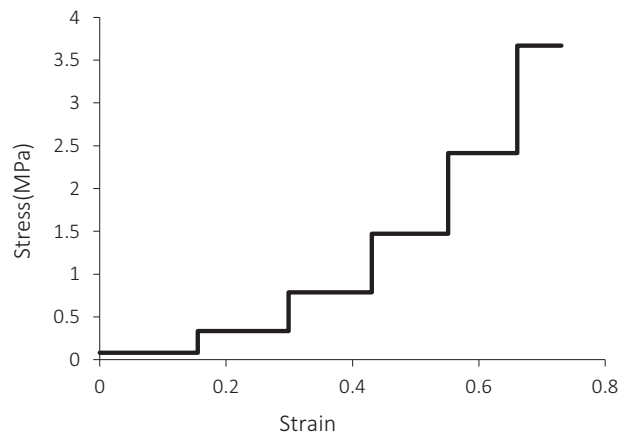


Figure 6. Analytical behaviour of GHS in Y-direction, using Equations (7) and (9).

Downloaded by [31.29.35.203] at 06:58 21 May 2015

structure perpendicular to the longitudinal direction and L is the structure height in longitudinal direction (direction of collision). According to the dimensions of honeycomb, the energy equation of Equation (15) can be rewritten as

$$U = 2bl \cos(\phi) (15c + 16l \sin(\phi)) \sum_{i=1}^6 \sigma_{p_i} \varepsilon_{d_i} \quad (16)$$

where σ_{p_i} is calculated for PHM as

$$\sigma_{p_i} = \left(\frac{\sigma_u}{n+2} \right) \frac{d_i^2}{(c + l \sin(\phi)) (l - d_i) \sin(\phi)} \quad (17)$$

and for EPPM as

$$\sigma_{p_i} = \left(\frac{\sigma_y}{2} \right) \frac{d_i^2}{(c + l \sin(\phi)) (l - d_i) \sin(\phi)} \quad (18)$$

The cell volume and mass are

$$V_c = db(4l + 2c) \quad (19)$$

$$m_c = \rho_s db(4l + 2c) \quad (20)$$

The structure has 6 rows and 15 cells in each row. Since the thickness of each row is different in this structure, the mass of entire structure is

$$m = \rho_s b(32l + 23c) \sum_{i=1}^6 d_i \quad (21)$$

An important parameter in the design of energy absorbers is the specific energy of structure, which is

$$e = \frac{U}{m} = \frac{2bl \cos(\phi) (15c + 16l \sin(\phi)) \sum_{i=1}^6 \sigma_{p_i} \varepsilon_{d_i}}{\rho_s b(32l + 23c) \sum_{i=1}^6 d_i} \quad (22)$$

A numerical analysis through FEM is conducted to validate the driven analytical results.

4. Validation of analytical equations

In order to validate the analytical equations obtained and comparing the results of equations based on two different material models, energy absorption of GHSs made of five various grades of aluminium is simulated in ABAQUS/CAE. In each problem, the structure is applied to a specific kinetic energy. The FEM of aluminium 1100-O of GHS is demonstrated in Figure 7. Hourglass controlled, four nodes, reduced integration shell elements (S4R) are used to mesh the structure, and rigid bilinear quadrilateral elements (R3D4) are used to mesh plate A

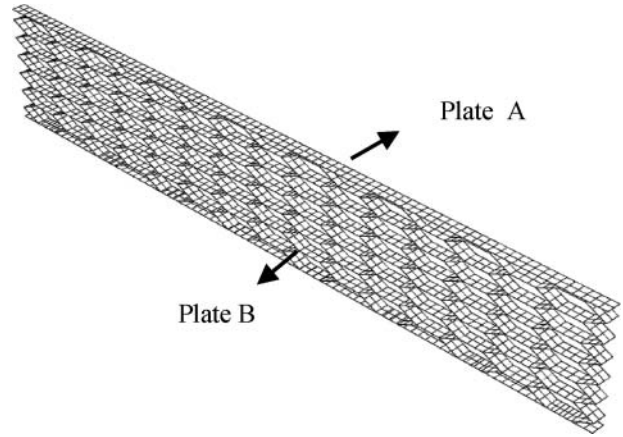


Figure 7. FE model of GHS.

and plate B. The GHS is thin-walled and the S4R element can be used. The boundary conditions are defined by constraining the discrete rigid plate, A, to move only in the Y -plane and by fixing all the rotational and translational degrees of freedom of the discrete rigid plate, B. Interaction properties are imposed using a general contact condition for contact of rows and surface-to-surface kinematic contact conditions between the top-element-based surface of the structure and the rigid plate, A. A penalty contact condition with friction tangential behaviour is applied between the bottom-element-based surface of the structure and the rigid plate, B. In this module, the coefficient of friction is equal to 0.2. Individual rows are attached to each other by Tie module.

In this simulation, the plateau-stress-locking strain diagram of the structure obtained from numerical solution is compared to analytical results for each material model. In addition, the numerical value of energy absorption is compared to that of analytical method for each material model. The geometrical characteristics of the structure are shown in Table 1. The material characteristics of utilised aluminium and the value of kinetic energy applied to the structure for PHM and EPPM are represented in Tables 2 and 3, respectively.

Table 1. Geometrical characteristics of the structure.

For AL-6061-O, AL-7075, AL-5052, AL 1100-O	For AL-2024	Geometric parameter
2.7 mm	2.7 mm	c
2.5 mm	2.5 mm	l
0.35 mm	0.6 mm	d_1
0.3 mm	0.499 mm	d_2
0.25 mm	0.399 mm	d_3
0.2 mm	0.299 mm	d_4
0.15 mm	0.2 mm	d_5
0.1 mm	0.1 mm	d_6
63°	63°	ϕ

Table 2. Material characteristics of different aluminium and kinetic energy applied to the structure for power hardening model.

Aluminium grade	K (MPa) [11]	n [11]	S_{ut} (MPa) [17]	Applied Kinetic energy (J)
1100-O	180	0.2	137	1.384
6061-O	205	0.2	150	0.555
5052-O	210	0.13	172	0.705
7075-O	400	0.17	290	1.185
2024-T4	690	0.16	437	2.04

Table 3. Material characteristics of different aluminium and kinetic energy applied to the structure for elastic–perfectly plastic model.

Aluminium grade	S_y (MPa) [17]	Applied kinetic energy (J)
1100-O	34.47	0.784
6061-O	55.15	0.38
5052-O	89.63	0.6
7075-O	103.42	0.71
2024-T4	324.05	2

Due to the above-mentioned material properties, the plastic behaviour based on the two mentioned material models is defined for each row individually. The velocity of the plate A is assigned to its reference point using a pre-defined field. The FE problem is solved by dynamic/explicit solver.

5. Experimental test

In order to validate the numerical simulation method in ABAQUS software, an experimental test has been conducted as the falling a weight with low velocity on a GHS. Our experimental model is a 6061-O aluminium GHS. This structure has six rows with different thicknesses. The rows are formed by ramrod and matrix, and then glued to each other by adhesive film. The thickness of the first to sixth rows is 1.6, 1.27, 1.016, 0.8125, 0.635 and 0.508 mm, respectively. For this model, $c = 15$, $l = 12$, $b = 28.5$ mm, and the height and width are 130 and 130 mm, respectively. This structure is designed and produced according to the production facilities, as demonstrated in Figure 8.

The rows of this structure have been formed by using punch and die, and have been attached to each other by means of an adhesive film. To determinate the characteristics of this alloy for a more precise analysis, the materials of all of the six thicknesses have been analysed under a tension test using Santam machine. The stress–strain diagram of the uniaxial tensile tests on the standard specimens of AL-6061-O plate has been sketched to determine each row material properties with the loading rate of 5 mm min^{-1} . The mechanical characteristics of each row

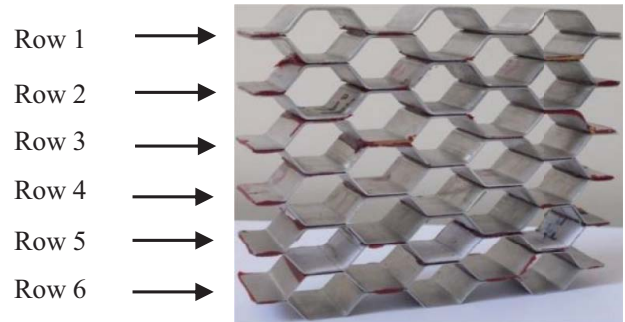


Figure 8. Testing sample of six-row graded honeycomb structure.

have been listed in Table 4. It is noteworthy that the density and Poisson ratio of this aluminium are 2700 kg m^{-3} and 0.33, respectively. The mechanical properties obtained are used to define the material properties in FE simulation. Low-velocity impact test has been performed by drop-hammer test device (Figure 9). In this test, 99 J kinetic energy was applied to the GHS. A system of 9776.6 g has dropped from a 1.2 m height. Due to the existence of several sources of loss such as friction, the velocity of the mass has been determined as 4.5 m s^{-1} by a speedometer while striking the sample. Moreover, the acceleration of the block has been recorded during the impact to the structure and energy absorption by an accelerometer. This accelerometer records the mass acceleration in each $13 \mu\text{s}$ and can measure maximum 100 g. By multiplying the value of acceleration by the mass of the system, the reaction force of the structure can be computed, while the deformation of the structure is calculated

Table 4. Mechanical properties of different thicknesses of AL6061-O plate.

Thickness (mm)	E (GPa)	n	K (MPa)	e_f (%)	S_{ut} (MPa)	S_y (MPa)
1.6	68.28	0.213	202.77	23.76	131.39	51.59
1.27	66.98	0.245	242.66	25.142	141	51.92
1.016	62.5	0.291	220.8	25.168	131	50.7
0.8125	63.51	0.229	205.6	30.72	141	50
0.635	64.3	0.247	228	27.06	134	48.15
0.508	66.81	0.303	217.27	31.092	124	53



Figure 9. Drop-weight test device and the accelerometer.

by two numerical integrals from the acceleration value. Based on these results, force–displacement diagram was sketched. The fixture of test specimen is shown in Figure 10.

5.1. Numerical simulation

Regarding the material and geometrical characteristics of the structure, the mass and velocity of the weight, loading and boundary conditions, the experimental test on the sample has been simulated in ABAQUS software. The FE model made of aluminium 6061-O of GHS is demonstrated in Figure 11. The dropped mass and the structure base are modelled by plates A and B, respectively. Hour-glass controlled, eight nodes, reduced integration linear brick elements (C3D8R) are used to mesh the structure, and rigid bilinear quadrilateral elements (R3D4) are used to mesh plate A and plate B, respectively. The structure wall is nearly thick here and the C3D8R element is used. The boundary conditions are defined by constraining the



Figure 10. Test specimen fixture.

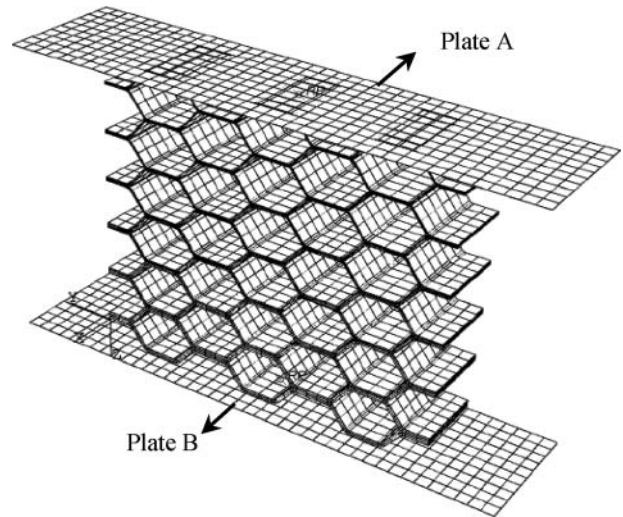


Figure 11. FE model of GHS.

discrete rigid plate, A, to move only in the Y -plane and by fixing all the rotational and translational degrees of freedom of the discrete rigid plate, B. Interaction properties are imposed using a general contact condition for contact of each row and surface-to-surface kinematic contact conditions between the top-element-based surface of the structure and the rigid plate, A. A penalty contact condition with friction tangential behaviour is applied between the bottom-element-based surface of the structure and the rigid plate, B. In this module based on test condition, the coefficient of friction is considered equal to 0.6. The adhesive film between the rows absorbs energy by converting the applied energy into strain energy. Hence, the glue is simulated by cohesive behaviour using general contact interaction. The velocity of the plate A is assigned to its reference point using predefined field. Using the measured material properties, the plastic behaviour of AL-6061O is defined using PHM for each row individually. The FE problem is solved by dynamic/explicit solver.

In this simulation, the reaction force–deformation diagram of the structure obtained from numerical solution is compared to the analytical and experimental results.

6. Optimisation

The crashworthiness of structures under impact load can be improved by using optimisation methods. Horstemeyer et al. [10] used multi-objective optimisation methods with FE analysis in the lightweight design for side-impact crashworthiness, considering two different criterions. Based on the results, the new injury-based design metric was much safer than the new energy absorption design metric. A genetic algorithm which is inspired from nature and applied to study the optimisation of complex systems is used here. In this approach, the search would continue

by using genetic functions to the point of obtaining better or even the best samples. One of the most important characteristics of these algorithms is the possibility of parallel processing [9]. Another optimisation algorithm is the sequential quadratic programming (SQP) in which the objective function is minimised by nonlinear constraints. This method is an iterative one for nonlinear optimisation. SQP methods are used on problems for which the objective function and the constraints are twice continuously differentiable. SQP methods solve a sequence of optimisation sub-problems, each of which optimises a quadratic model of the objective subject to a linearisation of the constraints. If the problem is unconstrained, then the method reduces to Newton's method for finding a point where the gradient of the objective vanishes. If the problem has only equality constraints, then the method is equivalent to applying Newton's method to the first-order optimality conditions, or Karush–Kuhn–Tucker conditions, of the problem [6]. In the current study, the initial structure consists of 6 cells in Y -direction and 15 cells in X -direction. The geometrical characteristics are mentioned in Table 1. The structure is subjected by a rigid plane with a mass of 1 kg and 1.664 m s^{-1} initial velocity. The purpose of optimisation here is the minimising of the mass ratio to the absorbed energy of the structure. For this purpose, SQP and genetic algorithms are utilised in MATLAB software with the objective function of the mass ratio to absorbed energy. According to Equation (18), the objective function is the mass ratio to the absorbed energy of the structure and the design parameters are as given in Table 5. Moreover, the design variable vector (\mathbf{X}) with nine elements is defined in this table.

For both algorithms, the optimisation problem is defined as

$$\min \left[\frac{m(\mathbf{X})}{U(\mathbf{X})} \right]$$

$$\text{s.t. } m = 0.0012 \text{ kg and } \frac{x(i)}{x(3)} < 0.25, \text{ for } i = 1, 3, 4, 5, 6, 7, 8$$

$$\mathbf{lb} \leq \mathbf{X} \leq \mathbf{ub}$$

Table 5. Design variables in optimisation problem.

Design variable (\mathbf{X})	Geometric parameter
$x(1)$	d_1
$x(2)$	c
$x(3)$	l
$x(4)$	d_2
$x(5)$	d_3
$x(6)$	d_4
$x(7)$	d_5
$x(8)$	d_6
$x(9)$	ϕ

The upper and lower limits of the variables are equal to the vectors \mathbf{ub} and \mathbf{lb} as

$$\mathbf{lb} = [0.0005; 0.0025; 0.002; 0.0004; 0.0003; 0.0002; 0.0001; 0.00005; 1.1] \\ (\text{mm}, \text{mm}, \text{mm}, \text{mm}, \text{mm}, \text{mm}, \text{mm}, \text{mm}, \text{rad})$$

$$\mathbf{ub} = [0.0006; 0.003; 0.0025; 0.0005; 0.0004; 0.0003; 0.0002; 0.0001; 1.3] \\ (\text{mm}, \text{mm}, \text{mm}, \text{mm}, \text{mm}, \text{mm}, \text{mm}, \text{mm}, \text{rad})$$

(23)

The optimisation is conducted by two genetic and SQP algorithms and their results are compared to each other. In genetic algorithm, a generation of 30 and two stopping criteria are applied as

- (1) a maximum number of 100 generations,
- (2) the number of continuous generations without a change in optimum point reaches 20.

A constraint and function tolerance of 10^{-9} is applied. In SQP method, the constraint and function tolerance equal to 10^{-6} and the start point equals to lower limit (\mathbf{lb}) is considered.

6.1. Numerical analysis

To evaluate the optimisation results, the optimised structure obtained is simulated by ABAQUS/CAE. The initial and optimised models are simulated and their energy absorption values are compared. The structure has a height of 17.16 mm and a width of 76.4 mm. In both models, the material used in the structure is aluminium 1100-O with the density of 2700 kg m^{-3} . Geometrical parameters of this simulation are based on the genetic algorithm results. It is noteworthy that the power hardening material and EPPM with aluminium are utilised and the rigid plane A collides to the structure with 1.791 m s^{-1} initial velocity. The rest of numerical simulation conditions are as mentioned in Section 4.

7. Results and discussion

In numerical simulation, the stress is calculated by dividing the reaction force of lower plate to its cross section and the strain is calculated by dividing the structure deformation to the initial length of the entire structure. According to the conducted numerical solution, the plateau stress-locking strain diagrams of two material models for aluminium with different grades are shown in Figure 12. Moreover, the maximum difference between numerical and analytical results for PHM and EPPM is represented in Tables 6 and 7, respectively. PHM denotes power hardening material model and EPPM denotes elastic-perfectly plastic material model in the following figures.

It is seen that the values obtained for plateau stress and locking strain from the represented analytical equations

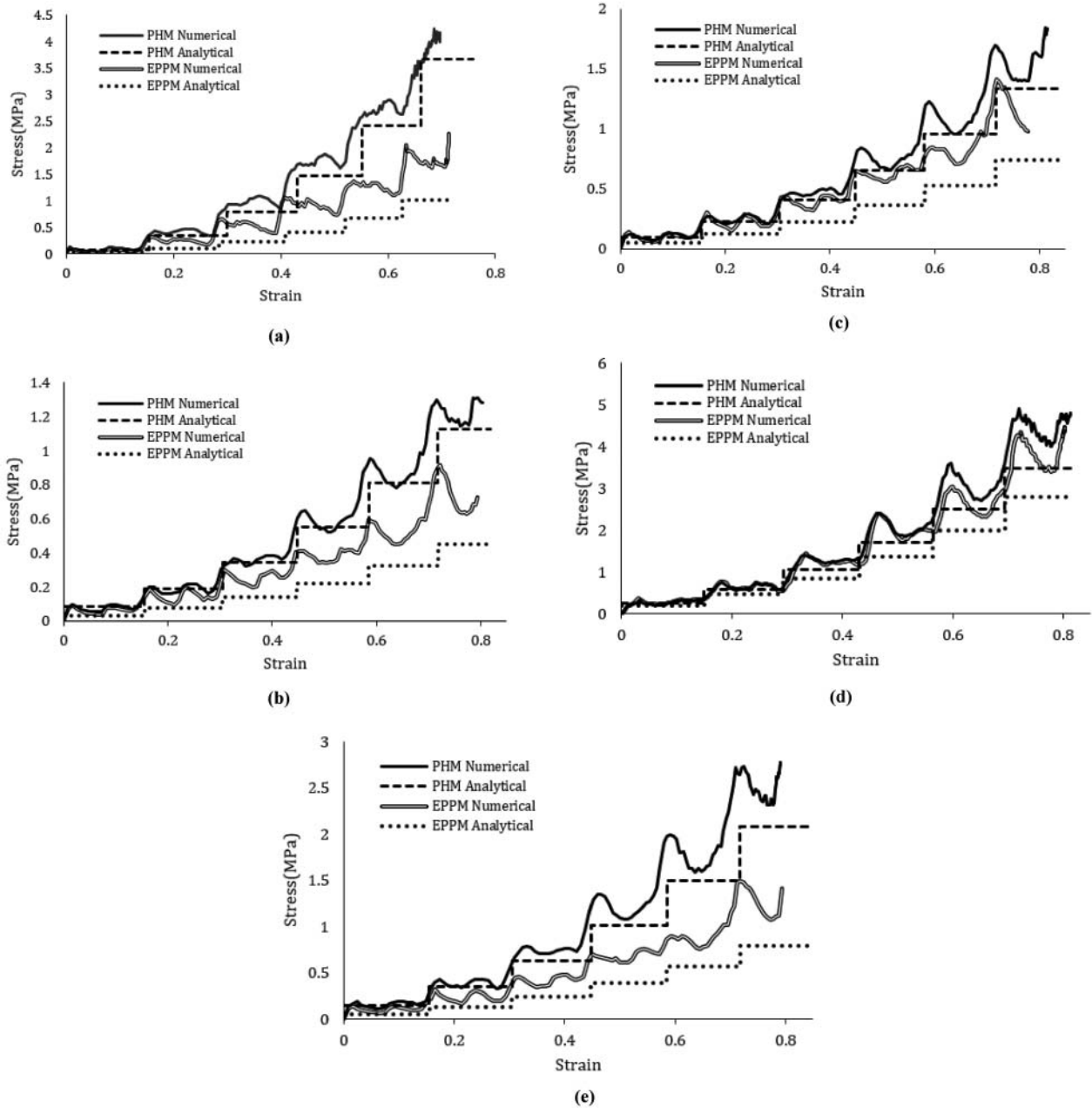


Figure 12. Stress–strain diagram for graded honeycomb structure made of different grades of aluminium: (a) 1100-O, (b) 6061-O, (c) 5052-O, (d) 7075-O and (e) 2024-T4.

Table 6. Analytical and numerical plateau stresses for different types of aluminium for PHM.

Aluminium grade	Numerical stress (MPa)	Analytical stress (Equation (7)) (MPa)	Maximum difference (%)
1100-O	3.97	3.66	7.72
6061-O	1.14	1.13	0.8
5052-O	1.4	1.33	5
7075-O	2.31	2.08	9.9
2024-T4	3.89	3.51	10.58

Table 7. Analytical and numerical plateau stresses for different types of aluminium for EPPM.

Aluminium grade	Numerical stress (MPa)	Analytical stress (Equation (4)) (MPa)	Maximum difference (%)
1100-O	1.65	1.01	38.78
6061-O	0.63	0.452	28.25
5052-O	0.987	0.735	25.53
7075-O	1.07	0.794	25.79
2024-T4	3.42	2.79	18.42

for PHM model have more appropriate congruence rather than EPPM model with numerical results. The maximum difference between numerical and analytical of plateau stress for PHM model is 10.58%; however, for EPPM, it is 38.78%. Analytical equations based on power hardening decrease the difference between the numerical and analytical results compared with those based on elastic–perfectly plastic behaviour. It, however, reasonably well captured the trend and pattern of the FE curve. With the conducted validation, the plateau stress equation based on PHM model can be utilised in deriving the equation of absorbed energy by the structure. Based on the kinetic energy applied to the structure, the analytical and numerical energy absorption values of structures with different aluminium grades for PHM and EPPM are compared in Figures 13 and 14, respectively. In addition, the difference between numerical and analytical absorbed energies for two material models is represented in Tables 8 and 9.

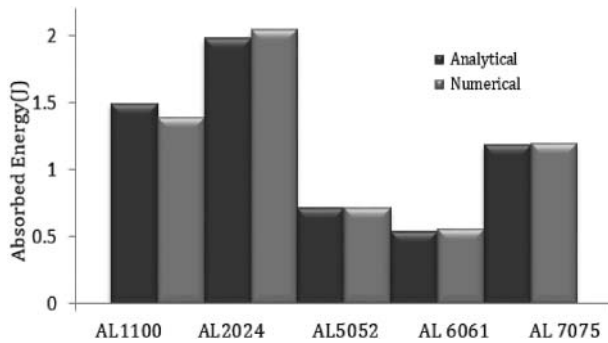


Figure 13. Comparing of analytical and numerical absorbed energies of GHS with different types of aluminium for PHM.

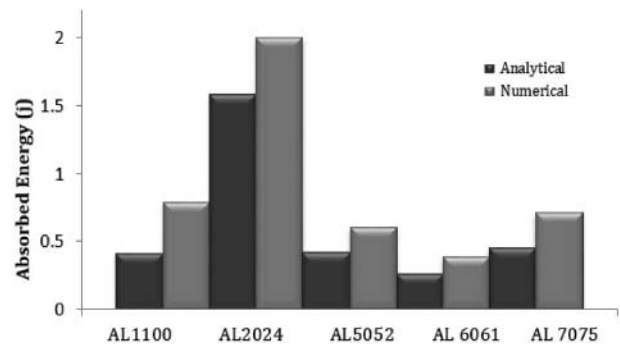


Figure 14. Comparing of analytical and numerical absorbed energies of GHS with different types of aluminium for EPPM.

It is observed that the numerical and analytical results for PHM indicate more proper congruence rather than EPPM model. The maximum difference between numerical and analytical absorbed energies for PHM is 6.4%; however, for EPPM it is 48.08%. Figure 12 shows that the analytical absorbed energy obtained is properly close to the numerical results, which shows that the PHM model analytical equations can be utilised in deriving stress–strain diagram and finding the absorbed energy by the structure. Based on the above comparison, the derived analytical equations for PHM (Equations (7) and (13)) show the real behaviour of material and then they are more useful and applicable than EPPM equations. Therefore, the PHM equations can be used for SAE optimisation of the GHS. In this simulation, the hourglass and friction loss of energy are 0.28% and 0.27% of the total internal energy, respectively. These amounts are lower than 5%; therefore, these energies can be neglected.

In the experimental test, the force–displacement diagram of the structure under the impact load with low

Table 8. Analytical and numerical absorbed energies for different types of aluminium for PHM.

Aluminium grade	Numerical AE (J)	Analytical AE (Equation (13)) (J)	Difference (%)
1100-O	1.385	1.48	6.4
6061-O	0.555	0.537	3.2
5052-O	0.705	0.704	3.2
7075-O	1.185	1.18	0.1
2024-T4	2.04	1.97	0.4

Table 9. Analytical and numerical absorbed energies for different types of aluminium for EPPM.

Aluminium grade	Numerical AE (J)	Analytical AE (Equation (13)) (J)	Difference (%)
1100-O	0.784	0.407	48.08
6061-O	0.38	0.255	32.89
5052-O	0.6	0.415	30.8
7075-O	0.71	0.448	36.9
2024-T4	2	1.57	21.3

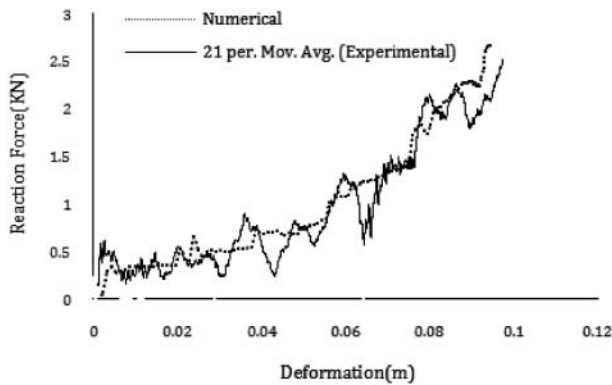


Figure 15. Force–displacement diagram of graded honeycomb structure for experimental test and numerical solution.

velocity has been demonstrated in Figure 15, according to the information obtained from the experimental test and numerical simulation. Furthermore, the deformed models of the structure after the experimental test and numerical simulation are compared in Figure 16.

Regarding Figures 15 and 16, the numerical results retain an acceptable accordance with the experimental results, in a way that the maximum error between the reaction force of experimental and numerical results is 5.4%. Hence, the numerical simulation method and the applied parameters in this simulation are validated.

According to SAE optimisation, the developed genetic algorithm stopped with the second stopping criteria after

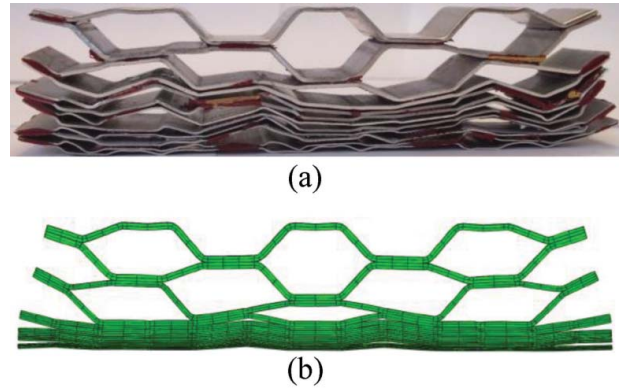


Figure 16. A deformed schema of the graded honeycomb structure obtained from (a) experimental test and (b) numerical solution.

31 iterations. The ratio of mass to absorbed energy is obtained as $7.475 \times 10^{-4} \text{ kg J}^{-1}$. On the other hand, the SQP algorithm stopped after 20 iterations with the constraint and function tolerance criteria. The ratio of mass to absorbed energy is obtained as $8.088 \times 10^{-4} \text{ kg J}^{-1}$. Optimisation results based on two algorithms are represented in Table 10.

By comparing the results obtained from genetic and SQP algorithms, it is seen that the ratio of mass to absorbed energy for the genetic algorithm is lower than that of the SQP, and then the former would be considered as the optimum choice. The absorbed energy by initial

Table 10. Design parameters obtained from genetic and SQP algorithms.

Design variable	Initial value (mm)	Optimised value by GA (mm)	Optimised value by SQP (mm)
l (mm)	2.5	2.466	2.47
c (mm)	2.7	2.96	2.94
t_1 (mm)	0.6	0.599	0.5826
t_2 (mm)	0.499	0.499	0.4868
t_3 (mm)	0.399	0.4	0.3868
t_4 (mm)	0.299	0.299	0.286
t_5 (mm)	0.2	0.1449	0.186
t_6 (mm)	0.1	0.0692	0.0899
ϕ (°)	63	54.43	55.4
AE (J)	1.388	1.6053	1.4837
Iterations	–	31	20

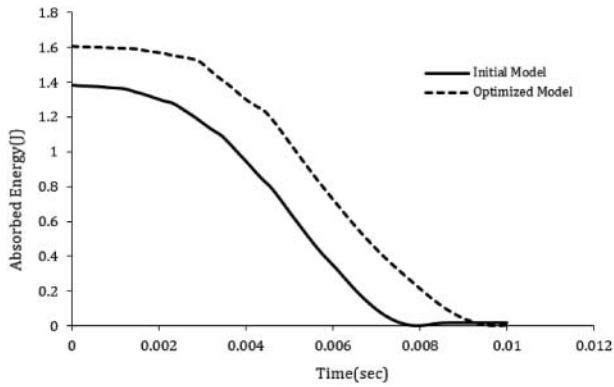


Figure 17. Diagram of kinetic energy changes for the initial and optimised models as a function of time.

structure and optimum one are 1.388 and 1.6053 J, respectively. Consequently, the capacity of absorbing energy increases about 18%. Based on the numerical simulation results, a history of the complete absorption of kinetic energy by GHS structure is demonstrated in Figure 17 for the initial and optimised models.

As it is observed, the initial structure absorbed the amount of 1.388 J, while the optimised one completely absorbed 1.6053 J kinetic energy. The optimisation results have appropriate congruence with simulation results. Increasing the duration of absorbing energy is an advantageous parameter in energy absorber design. In other words, the optimised structure could absorb more energy in a longer period of time. Hence, the optimisation algorithm can increase both energy capacity and duration of energy absorbing.

The represented values of absorbed energy in Sections 4 and 6 considering the dimensions of the modelled GHS are based on the banana peel structure. Applying optimisation algorithms and the represented analytical equations with enlarging the dimensions of GHS and filling it with foam prove that the energy absorption can be increased. Using the introduced honeycomb structure, the analytical equations and optimisation algorithm, the energy absorption can be increased. This kind of energy absorber can be used for elevators, infant car seat and helicopter seat for improving the crashworthiness in emergency conditions.

8. Conclusions

Based on the obtained plateau stress equation and the locking strain equation, the specific absorbed energy (SAE) equation for GHS was derived. To validate and compare the derived equations for two material models, an FE simulation on absorbing energy of GHS under in-plane impact load was performed. Comparison shows that the PHM have more appropriate congruence rather than the EPPM one with numerical results. As previously mentioned, the maximum difference between the numerical and analytical plateau

stresses for PHM model is 10.58%; however, for EPPM, this value is 38.78%. Besides, the maximum difference between the numerical and analytical absorbed energies for PHM model is 6.4%, while this value has been measured to be 48.08% for EPPM. Analytical equations based on power hardening reduce the difference between the numerical and analytical results compared with those based on EPPM. The numerical results obtained are of an acceptable accordance with the experimental ones in such a way that the maximum measured error between the reaction force of experimental and numerical results is 5.4%. According to the optimisation results, the structure capacity of absorbing energy increases by 18% compared to that of the primary model. In fact, the graded status of the structure and the in-plane loading could reduce the applied impact load to the protected body and decrease the cost and physical damage compared to non-graded structure and out-of-plane loading. Generally and according to the increasing application of GHSS, the represented analytical equations based on PHM and optimisation method can be utilised to reduce the ratio of structure mass to absorbed energy in in-plane impact load conditions.

Disclosure statement

No potential conflict of interest was reported by the authors.

References

- [1] S. Adibnazari and H. Mehrabi, *Effect of cell size change on honeycomb structure equivalent mechanical property*, 10th Iran Aerospace conference (AERO2011), Tarbiat Modares University, Tehran, 2011.
- [2] A. Ajdari, H. Nayeb-Hashemi, and A. Vaziri, *Dynamic crushing and energy absorption of regular, irregular and functionally graded cellular structures*, Int. J. Solids Struct. 48 (2011), pp. 506–516.
- [3] M. Asadi, H. Shirvani, E. Sanaei, and M. Ashmead, *A simplified model to simulate crash behavior of honeycomb*, Proceedings of the International Conference on Advanced Design and Manufacture, Harbin, (2006).
- [4] F.P. Beer, E.R. Johnston, J.T. DeWolf, and D.F. Mazurek, *Mechanics of Materials*, McGraw-Hill, New York, NY, 2012.
- [5] T. Bitzer, *Honeycomb Technology: Materials, Design, Manufacturing, Applications and Testing*, 1st ed., Chapman and Hall, New York, NY, 1997.
- [6] F.J. Bonnans, C.J. Gilbert, C. Lemaréchal, and C.A. Sagastizábal, *Numerical Optimization: Theoretical and Practical Aspects*, Springer, London, 2006.
- [7] S. Deqiang, Z. Weihong, and W. Yanbin, *Mean out-of-plane dynamic plateau stresses of hexagonal honeycomb cores under impact loadings*, Compos. Struct. 92 (2010), pp. 2609–2621.
- [8] L.J. Gibson and M.F. Ashby, *Cellular Solids: Structures and Properties*, 2nd ed., Cambridge University Press, Cambridge, 1997.
- [9] D.E. Goldberg and M.P. Samadani, *Engineering optimization via genetic algorithm*, 9th Conference of Electronic Computation (ASCE), University of Alabama, Birmingham, AL, 1986.

- [10] M. Horstemeyer, X.C. Ren, H. Fang, E. Acar, and P.T. Wang, *A comparative study of design optimization methodologies for side-impact crashworthiness using injury-based versus energy-based criterion*, Int. J. Crashworthiness 14 (2009), pp. 125–138.
- [11] S. Kalpakjian, *Manufacturing Processes for Engineering Materials*, 2nd ed., Addison-Wesley, Boston, MA, 1995.
- [12] A.S. Khan and S. Huang, *Continuum Theory of Plasticity*, John Wiley, Hoboken, NJ, 1995.
- [13] J.C. Koch, *The laws of bone architecture*, Am. J. Anatomy 21 (1917), pp. 177–198.
- [14] M. Kojic and K.J. Bathe, *Inelastic Analysis of Solids and Structures*, Springer, London, 2005.
- [15] G. Liaghat and H. Sarailou, *Optimum design of honeycomb core under compression load*, Tech. Eng. J. Modarres 37 (2010), pp. 73–81.
- [16] G. Lu and T.X. Yu, *Energy Absorption of Structures and Materials*, Wood Head Publishing Limited & CRC Press, Boca Raton, FL, 2003.
- [17] T. Lyman, *Metals Handbook*, American Society of Metals, Metals Park, OH, 1966.
- [18] A. Muhammad, *Study of a compact energy absorber*, Ph.D. thesis, Iowa State University, 2007.
- [19] A. Muhammad, J. Hoffman, J. Clark, and S. Takak, *Modeling of Impact Response of Composite Graded Structure*, IMECE, Denver, CO, 2011.
- [20] A. Muhammad, S-i. Kim, and T. Matthews, *Modeling of a compact functionally graded cellular structure: A finite element study for medium and high strain rates*, Int. J. Mech. Mater. Des. 10 (2014), pp. 79–92.
- [21] A. Niknejad and G. Liaghat, *Experimental study of Polyorthan foam filler on hexagonal honeycomb structure behavior under axial load with constant rate*, 10th Iran Aerospace conference (AERO2011), Tarbiat Modarres University, Tehran, 2011.
- [22] S.D. Papka and S. Kyriakides, *In-plane compressive response and crushing of honeycomb*, J. Mech. Phys. Solids 42 (1994), pp. 1499–1532.
- [23] S.D. Papka and S. Kyriakides, *In-plane crushing of a polycarbonate honeycomb*, Int. J. Solids Struct. 35 (1998), pp. 239–267.
- [24] W. Prager and P.G. Hodge, *Theory of Perfectly Plastic Solids*, John Wiley, Hoboken, NJ, 1951.
- [25] K.S. Przemieniecki, *Theory of Matrix Structural Analysis*, McGraw-Hill, New York, NY, 1968.
- [26] D.W.A. Rees, *Basic Engineering Plasticity*, Elsevier, Amsterdam, 2006.
- [27] Y. Song, Z. Wang, L. Zhao, and J. Luo, *Dynamic crushing behavior of 3D closed-cell foams based on Voronoi random model*, Mater. Des. 31 (2010), pp. 4281–4289.
- [28] T.X. Yu and L.C. Zhang, *Plastic Bending: Theory and Applications*, Vol. 2, Series of Engineering Mechanics, World Scientific, Singapore, 1996.
- [29] Z. Zou, S.R. Reid, P.J. Tan, S. Li, and J.J. Harrigan, *Dynamic crushing of honeycombs and features of shock fronts*, Int. J. Impact Eng. 36 (2009), pp. 165–167.